

## Self-similar solution of a supercritical two-phase laminar mixing layer

J. Poblador-Ibanez\*, B.W. Davis, and W.A. Sirignano  
Department of Mechanical and Aerospace Engineering  
University of California, Irvine  
Irvine, CA 92697, USA

### Abstract

Previous works for a liquid suddenly contacting a gas at a supercritical pressure show the coexistence of both phases and the generation of diffusion layers on both sides of the liquid-gas interface due to thermodynamic phase equilibrium. A related numerical study of a laminar mixing layer between a liquid stream and a gas stream in the near field of the splitter plate suggests that mass, momentum and thermal diffusion layers evolve in a self-similar manner at very high pressures. In this paper, the high-pressure, two-phase, laminar mixing-layer equations are recast in terms of a similarity variable without further simplification of the fluid behavior. A liquid hydrocarbon and gaseous oxygen are considered. Free-stream conditions and a proper matching condition between the two phases at the liquid-gas interface are applied. To solve the system of equations, a non-ideal thermodynamic model based on the Soave-Redlich-Kwong equation of state and other high-pressure models is selected. A comparison with results obtained by directly solving the system of partial differential equations defining the laminar mixing layer behavior shows the validity of the similarity approach applied to non-ideal two-phase flows. Even when the gas is hotter than the liquid, condensation can occur at high pressures while heat conducts into the liquid.

---

\*Corresponding Author: poblador@uci.edu



## Introduction

Combustion chambers used in many engineering applications (e.g., power units, gas turbines or liquid-propellant rockets) are designed to operate at elevated pressures. That is, a thermodynamic regime is sought where less dissociation of the reaction products occurs and a better combustion efficiency and specific energy conversion are obtained. In many situations, the chamber pressure is well above the critical pressure of the liquid fuel that is being injected. Well-known fuels are based on hydrocarbon mixtures (e.g., diesel fuel, Jet A, RP-1) with critical pressures around 20 bar, while operating pressures may range from 25 to 40 bar in diesel engines or gas turbines and 70 to 200 bar in rocket engines.

The performance of the combustion reaction also depends on the rates of liquid fuel vaporization and mixing with the surrounding oxidizer. Therefore, understanding the physical phenomena involved in this process is necessary for a proper design of the injectors' shape and distribution, combustion chamber size, etc. At subcritical pressures, a clear distinction exists between liquid and gas phases, which allows for extensive experimental studies. However, for near-critical or supercritical pressures, experimental studies show that a thermodynamic transition occurs where the liquid and gas present similar fluid properties (e.g., compressibility) near the liquid-gas interface, which is suddenly immersed in a variable-density layer and is rapidly affected by turbulence [1, 2, 3, 4, 5, 6, 7, 8, 9].

Past works have described this behavior as a very fast transition of the liquid phase to a supercritical state, assuming that a two-phase behavior cannot be sustained under these thermodynamic conditions as suggested by experimental results where a gas-like turbulent structure is observed [10, 11]. But evidence of a two-phase behavior at supercritical pressures in multicomponent fluids exists based on a requirement of thermodynamic phase equilibrium at the liquid-gas interface [12, 13, 14, 15, 16, 17]. Some authors suggest caution at pressures near the critical pressure of the mixture, where the liquid-gas interface enters a continuum region of a few nanometers thickness [18, 19]. Accordingly, a two-phase behavior cannot exist, but diffusion around the interface occurs rapidly enough to reach diffusion layer thicknesses of the order of micrometers while phase equilibrium is well established [17].

There are further reasons that support the fact that liquid injection at supercritical pressures is still a two-phase problem. Surface tension forces are reduced but may still exist at very high pressures due to both phases presenting similar densities at the interface. Therefore, the aerodynamic effects on the liquid breakup process are enhanced [20]. Moreover, mixing causes the liquid viscosity to drop to gas-like values near the interface, reducing viscous damping of surface instabilities [21]. Altogether, fast growing instabilities associated with smaller wavelengths develop at the interface, which may cause a very fast atomization of the liquid jet with a cloud of very small droplets around it. Traditional experimental techniques have difficulties with visual penetration of dense sprays due to the scattering related to the large amount of small droplets and the intrinsic difficulties of variable-density fluids, thus making it difficult to distinguish between liquid and gas phases. Some new techniques have been able to penetrate dense sprays and show clear liquid structures (i.e., ligaments, lobes, bigger droplets) emerging from the liquid core, although they have not been tested yet in supercritical environments [22, 23].

The present work does not address the hydrodynamic instabilities that occur farther downstream as part of the atomization process. It focuses on the initial laminar mixing between the injected liquid and the gas before substantial growth of surface instabilities or transition to turbulence. Understanding how the mixing between both streams evolves is crucial to understand the beginning of high-pressure atomization and can also help create models to use as initial conditions for more complex numerical studies.

Davis et al. [24] present a two-dimensional numerical study involving the non-ideal two-phase laminar mixing layer equations and provide guidelines on the validity of these relations. Results are presented for a binary mixture where a liquid stream and a gas stream come together at the end of a splitter plate at various ambient pressures, ranging from subcritical to supercritical for the pure liquid. The liquid stream is initially composed of pure *n*-decane and the gas stream is pure oxygen. The mixing layer thickness grows to a few micrometers in the liquid phase and to tens of micrometers in the gas phase with downstream distance from the end of the splitter plate. At the same time, the interface reaches a near-steady solution sufficiently far away from the splitter plate. Most importantly, each individual configuration (i.e., each set of boundary conditions) shows signs of a self-similar behavior of the mixing layer evolution, even when the defined mixing layer equations involve non-ideal terms and are coupled to a non-ideal thermodynamic model involving a real-gas equation of state, thermodynamic fundamental principles and various high-pressure correlations. A self-similar behavior in this high-pressure environment is also suggested in Poblador-Ibanez



and Sirignano [17], although a non-ideal unsteady one-dimensional model is implemented.

Reducing the system of partial differential equations (i.e., mixing layer equations) to a system of ordinary differential equations in terms of a similarity variable is of special interest, not only because a simplified mathematical model describing the same phenomena is obtained, but also because of the fundamental analysis implied in the transformation. Similarity solutions have always been sought in classical fluid mechanics (e.g., the Blasius solution for flow over a flat plate or the Falker-Skan wedge flows), usually limited to incompressible flows. Some transformations are also available for compressible flows or flows with variable fluid properties, although simplifications are made to obtain a generic self-similar model (e.g., use of ideal-gas model). In general, these approaches are well documented in classical textbooks [25, 26]. For analyzing compressible or variable-density laminar shear layers, the focus is usually limited to single-phase configurations under ideal-gas assumptions with momentum and thermal mixing. Some works also include species mixing in their analysis [27].

In view of the discussed numerical results [17, 24], the non-ideal two-phase laminar mixing layer equations are recast in terms of a similarity variable, thus forming a system of ordinary differential equations. Boundary conditions and liquid-gas interface matching relations are provided, which allow for mass, momentum and energy transfer across the interface. Then, the self-similar model is coupled to a non-ideal thermodynamic model to close the system of equations. The self-similar solution is compared against the results from Davis et al. [24] at different problem configurations to assess the validity of the self-similar model.

### Laminar Mixing Layer Equations

The behavior of two parallel streams coming together at the edge of a splitter plate (see Figure 1) can be modeled under the boundary layer approximation after a transitional region [25]. For a sufficiently large Reynolds number, the flow begins to develop with the transverse velocity being much smaller than the streamwise velocity,  $v \ll u$ , and variations in the  $x$ -direction become negligible compared to variations in  $y$  (i.e.,  $\partial()/\partial x \ll \partial()/\partial y$ ). The transverse pressure gradient,  $\partial p/\partial y$ , is also negligible. Therefore, the solution for the transverse velocity is directly obtained from the continuity equation and not from the transverse momentum equation [17, 28]. For free-shear low-Mach number flows at high pressures without confining walls, pressure can be assumed constant ( $Dp/Dt = \partial p/\partial x = \partial p/\partial y = 0$ ). Furthermore, viscous dissipation and kinetic energy can be safely neglected in the energy equation.

Under these conditions, the steady-state governing equations written in non-conservative form describing the two-phase laminar mixing layer development of two non-ideal fluids (i.e., a liquid stream and a gas stream) are the continuity equation, Eq. (1), the streamwise momentum equation, Eq. (2), the species continuity equation, Eq. (3), and the energy equation, Eq. (4).

$$\frac{\partial}{\partial x}(\rho u) + \frac{\partial}{\partial y}(\rho v) = 0 \quad (1)$$

$$\rho u \frac{\partial u}{\partial x} + \rho v \frac{\partial u}{\partial y} = \frac{\partial}{\partial y} \left( \mu \frac{\partial u}{\partial y} \right) \quad (2)$$

$$\rho u \frac{\partial Y_1}{\partial x} + \rho v \frac{\partial Y_1}{\partial y} = \frac{\partial}{\partial y} \left( \rho D \frac{\partial Y_1}{\partial y} \right) \quad (3)$$

$$\begin{aligned} \rho u \frac{\partial h}{\partial x} + \rho v \frac{\partial h}{\partial y} &= \frac{\partial}{\partial y} \left( \frac{\lambda}{c_p} \frac{\partial h}{\partial y} \right) \\ &+ \frac{\partial}{\partial y} \left[ \left( \rho D - \frac{\lambda}{c_p} \right) (h_1 - h_2) \frac{\partial Y_1}{\partial y} \right] \end{aligned} \quad (4)$$

In this work, a binary configuration is implemented. That is, both fluid streams are initially pure components (e.g., a pure liquid hydrocarbon and a pure gas, such as oxygen). For simplicity, a Fickian form is used to represent mass diffusion in Eqs. (3) and (4). The governing equations are written in terms of the mass fraction of one mixture component,  $Y_1$ , where the relation  $Y_1 + Y_2 = 1$  defines the composition of the other species. Furthermore, the energy equation is rewritten as an enthalpy transport equation by making the substitution  $\lambda \nabla T = (\lambda/c_p) \nabla h - \sum_{i=1}^N (\lambda/c_p) h_i \nabla Y_i$ . Note that since the problem is diffusion-driven, fluid properties will vary as species and energy diffuse and cannot be assumed constant.



These steady-state equations are valid as long as the flow is laminar and surface instabilities are negligible. Davis et al. [24] provide some guidance for oxygen-hydrocarbon mixtures at various ambient pressures. It is shown that the quasi-parallel laminar region may exist up to a distance from the splitter plate of the order of  $\mathcal{O}(10^{-2} \text{ m})$  while keeping the mean flow velocity at 10 m/s and varying the velocity difference between both streams in the range of  $\Delta u = 0.3 - 5 \text{ m/s}$ . With this analysis, one of the main goals is to show the existence of a two-phase behavior before hydrodynamic instabilities become important.

### Similarity Transformation

The system of partial differential equations describing the problem (Eqs. (1), (2), (3) and (4)) can be transformed into a system of ordinary differential equations by using a proper similarity variable,  $\eta$ . The mapping follows  $(x, y) \rightarrow (\bar{x}, z) \rightarrow \eta$ , where the first transformation is

$$\bar{x} = x \quad ; \quad z = \int_0^y \rho dy' \quad (5)$$

In Eq. (5),  $y'$  is a dummy variable used for the integration and  $z$  is a density-weighted transverse coordinate following the Howarth-Dorodnitsyn transformation [26]. As shown in Figure 1, the interface between the two phases is placed at  $y = 0$ . To transform the original system of equations from  $(x, y) \rightarrow (\bar{x}, z)$ , the following relations between partial derivatives are obtained

$$\frac{\partial}{\partial x}() = \frac{\partial}{\partial \bar{x}}() + \left( \int_0^y \frac{\partial \rho}{\partial x} dy' \right) \frac{\partial}{\partial z}() \quad (6)$$

$$\frac{\partial}{\partial y}() = \rho \frac{\partial}{\partial z}() \quad (7)$$

The transformed transverse velocity is defined as

$$w = \rho v + u \int_0^y \frac{\partial \rho}{\partial x} dy' \quad (8)$$

Then, the velocity components can be related to the stream function for compressible flow,  $\Psi(\bar{x}, z)$ , as

$$u = \frac{\partial \Psi}{\partial z} \quad ; \quad w = -\frac{\partial \Psi}{\partial \bar{x}} \quad (9)$$

Here,  $w$  does not have units of velocity and can be considered as a convenient variable in the solution process.

This arrangement yields a system of partial differential equations in the  $(\bar{x}, z)$  space in terms of the compressible stream function, Eqs. (10)-(13). Note the continuity equation, Eq. (10), is identically satisfied.

$$\frac{\partial^2 \Psi}{\partial \bar{x} \partial z} - \frac{\partial^2 \Psi}{\partial z \partial \bar{x}} = 0 \quad (10)$$

$$\frac{\partial \Psi}{\partial z} \frac{\partial^2 \Psi}{\partial \bar{x} \partial z} - \frac{\partial \Psi}{\partial \bar{x}} \frac{\partial^2 \Psi}{\partial z^2} = \frac{\partial}{\partial z} \left( \rho \mu \frac{\partial^2 \Psi}{\partial z^2} \right) \quad (11)$$

$$\frac{\partial \Psi}{\partial z} \frac{\partial Y_1}{\partial \bar{x}} - \frac{\partial \Psi}{\partial \bar{x}} \frac{\partial Y_1}{\partial z} = \frac{\partial}{\partial z} \left( \rho^2 D \frac{\partial Y_1}{\partial z} \right) \quad (12)$$

$$\begin{aligned} \frac{\partial \Psi}{\partial z} \frac{\partial h}{\partial \bar{x}} - \frac{\partial \Psi}{\partial \bar{x}} \frac{\partial h}{\partial z} &= \frac{\partial}{\partial z} \left( \frac{\rho \lambda}{c_p} \frac{\partial h}{\partial z} \right) \\ + \frac{\partial}{\partial z} \left[ \left( \rho^2 D - \frac{\rho \lambda}{c_p} \right) (h_1 - h_2) \frac{\partial Y_1}{\partial z} \right] \end{aligned} \quad (13)$$

After this intermediate step, the self-similar transformation is taken by defining the similarity variable as in the Blasius solution for a flat plate [25], but where  $x$  is substituted by  $\bar{x}$  and  $y$  is substituted by  $z$  as

$$\eta = \frac{z}{\sqrt{2\bar{x}}} \quad (14)$$



The transformation from  $(\bar{x}, z) \rightarrow \eta$  requires the following relations between partial derivatives

$$\frac{\partial}{\partial z}() = \frac{1}{\sqrt{2\bar{x}}} \frac{\partial}{\partial \eta}() \quad (15)$$

$$\frac{\partial}{\partial \bar{x}}() = \frac{\partial}{\partial \bar{x}}() - \frac{1}{2} \frac{\eta}{\bar{x}} \frac{\partial}{\partial \eta}() \quad (16)$$

where  $\bar{\bar{x}} = \bar{x} = x$ .

A self-similar solution exists if  $\Psi/\sqrt{x}$ ,  $Y_1$  and  $h$  depend only on  $\eta$ . Therefore, it is imposed that  $\Psi = \sqrt{2\bar{x}}f(\eta)$ ,  $Y_1 = Y(\eta)$  and  $h = h(\eta)$ . Then, from Eq. (9), the velocity components read

$$u = \frac{df}{d\eta} = f'(\eta) \quad ; \quad w = \frac{1}{\sqrt{2\bar{x}}} \left( \eta f'(\eta) - f(\eta) \right) \quad (17)$$

where the  $()'$  operator applied to any variable  $a$  (i.e.,  $a'$ ) means  $da/d\eta$ . Second and third derivatives follow the same notation.

Rearranging Eqs. (11)-(13), a system of ordinary differential equations can be written as

$$(\rho\mu)f''' + (\rho\mu)'f'' + ff'' = 0 \quad (18)$$

$$(\rho^2 D)Y'' + (\rho^2 D)'Y' + fY' = 0 \quad (19)$$

$$\begin{aligned} & \left( \frac{\rho\lambda}{c_p} \right) h'' + \left( \frac{\rho\lambda}{c_p} \right)' h' \\ & + \left( \rho^2 D - \frac{\rho\lambda}{c_p} \right) (h_1 - h_2) Y'' \\ & + \left[ \left( \rho^2 D - \frac{\rho\lambda}{c_p} \right) (h_1 - h_2) \right]' Y' + fh' = 0 \end{aligned} \quad (20)$$

where single dependence on  $\eta$  is implicit in the relations.

Another requirement needed to achieve similarity relates to the thermodynamic model used to evaluate fluid properties and transport coefficients. For these variables to depend only on  $\eta$ , the thermodynamic model must ultimately depend on pressure, temperature (i.e., enthalpy) and mixture composition. The self-similar model relies on a constant pressure everywhere in the domain, while temperature and mixture composition will depend only on  $\eta$ .

The thermodynamic model implemented in this work is based on a volume-corrected Soave-Redlich-Kwong (SRK) cubic equation of state [29], which is able to represent non-ideal fluid states. The volumetric correction is needed to obtain accurate density predictions of high-density fluids (i.e., liquids), since the original SRK equation of state [30] presents liquid density errors of up to 20% when compared to experimental values [20, 31]. The volume-corrected SRK equation of state is used, together with high-pressure correlations, to evaluate fluid properties and transport coefficients [32, 33, 34]. Details on the development and implementation of this thermodynamic model can be found in Davis et al. [24].

## Boundary Conditions

The governing equations representing the non-ideal two-phase laminar mixing layer have been reduced to a system of ordinary differential equations, Eqs. (18)-(20), which depends only on the similarity variable,  $\eta$ . To solve this system of equations, proper boundary conditions need to be imposed. These can be divided into freestream conditions for each individual fluid and interface matching conditions between both fluid streams.

The self-similar transformation is defined such that the liquid-gas interface does not move ( $V_\Gamma = 0$ ) and is located at  $y = z = \eta = 0$ . The reasonableness of this approximation has been shown by Davis et al. [24]. Positive values of  $\eta$  define the gas stream, while negative values of  $\eta$  represent the liquid stream. Following this definition, freestream boundary conditions for  $f$ ,  $Y$  and  $h$  become

$$\begin{aligned} f'(+\infty) &= u_G \quad ; \quad f'(-\infty) = u_L \\ Y(+\infty) &= Y_G \quad ; \quad Y(-\infty) = Y_L \\ h(+\infty) &= h_G \quad ; \quad h(-\infty) = h_L \end{aligned} \quad (21)$$



At  $\pm\infty$ , both streams are pure components. Thus, if  $Y_1$  is chosen to represent the pure gas species,  $Y_G = 1$  and  $Y_L = 0$  in Eq. (21).

Across the interface, which is denoted by  $\Gamma$ , the streamwise velocity component and the tangential stress are continuous. These conditions are expressed in the self-similar space as

$$f'_g(0) = f'_l(0) = U_\Gamma \quad (22)$$

$$\frac{f''_l(0)}{f''_g(0)} = \frac{(\rho\mu)_{g,\Gamma}}{(\rho\mu)_{l,\Gamma}} \quad (23)$$

Therefore,  $f'$  is continuous across the interface while a jump in the second derivative,  $f''$ , exists for  $(\rho\mu)_{g,\Gamma} \neq (\rho\mu)_{l,\Gamma}$ . Another condition for  $f$  is obtained from the mass balance across the interface. Since the interface location is assumed to remain fixed, the net mass flux across the interface reads

$$\dot{\omega} = (\rho v)_{g,\Gamma} = (\rho v)_{l,\Gamma} \quad (24)$$

Eq. (24) is expressed in terms of  $f(\eta)$  as

$$\dot{\omega} = -\frac{1}{\sqrt{2x}}f_g(0) = -\frac{1}{\sqrt{2x}}f_l(0) \quad (25)$$

which shows that  $f$  is also continuous across the interface (i.e.,  $f_g(0) = f_l(0)$ ).

Finally, expressions for the species mass balance and energy balance at the interface are needed. Eqs. (26) and (27) express these relations in the self-similar space in terms of  $f(\eta)$ ,  $Y(\eta)$  and  $h(\eta)$  as

$$\begin{aligned} & (f(0)Y(0))_g + (\rho^2 DY'(0))_g \\ & = (f(0)Y(0))_l + (\rho^2 DY'(0))_l \end{aligned} \quad (26)$$

$$\begin{aligned} -f_g(0)(h_g(0) - h_l(0)) &= \left(\frac{\rho\lambda}{c_p}h'(0)\right)_g - \left(\frac{\rho\lambda}{c_p}h'(0)\right)_l \\ &+ \left[\left(\rho^2 D - \frac{\rho\lambda}{c_p}\right)(h_1 - h_2)Y'(0)\right]_g \\ &- \left[\left(\rho^2 D - \frac{\rho\lambda}{c_p}\right)(h_1 - h_2)Y'(0)\right]_l \end{aligned} \quad (27)$$

A thermodynamic closure is needed to fully evaluate the interface solution of the system of ordinary differential equations. For that purpose, thermodynamic phase equilibrium is used. Chemical potentials of each species on both sides of the liquid-gas interface are imposed to be the same. This condition is expressed through an equality in fugacity for each species [30, 32] as  $f_{li}(T_l, p_l, X_{li}) = f_{gi}(T_g, p_g, X_{gi})$ . Under constant pressure across the interface, phase equilibrium can be expressed using the fugacity coefficient,  $\Phi_i \equiv f_i/pX_i$ , as

$$X_{li}\Phi_{li} = X_{gi}\Phi_{gi} \quad (28)$$

Note that liquid and gas compositions are only the same at the mixture critical point. Therefore, phase equilibrium shows that  $Y$  and  $h$  are discontinuous across the interface, as well as other fluid properties (e.g., density).

Since the thickness of the interface is of the order of  $\mathcal{O}(10^{-9} \text{ m})$  [18, 19] and diffusion layers in non-ideal high-pressure conditions quickly reach thicknesses of the order of  $\mathcal{O}(10^{-6} \text{ m})$  [17, 24], the interface thickness is neglected and temperature is assumed to be continuous across the interface (i.e.,  $T_g(0) = T_l(0) = T_\Gamma$ ). The very fast adjustment of the interface solution supports the thermodynamic equilibrium assumption [17, 24].



## Results

The system of ordinary differential equations, Eqs. (18)-(20), is solved numerically as follows. Instead of solving a third-order differential equation, Eq. (18) is split into a first-order differential equation to solve for  $f$ , Eq. (29), and a second-order differential equation to solve for  $f'$ , Eq. (30). Two new variables are introduced:  $g_1 = f'$  and  $g_2 = f$ .

$$g_2' = g_1 \quad (29)$$

$$(\rho\mu)g_1'' + (\rho\mu)'g_1' + g_2g_1' = 0 \quad (30)$$

Eqs. (19), (20), (29) and (30) are discretized using a second-order finite difference scheme and solved using a tri-diagonal matrix solver. Since the system of equations is highly coupled, some iterations are needed before reaching a converged solution.

The interface solution is also updated at every iteration. The streamwise momentum matching conditions, Eqs. (22) and (23), are combined numerically to solve for  $U_\Gamma$  or  $f'(0)$ . On the other hand, Eqs. (26), (27) and (28) form a closed system that can be solved at every iteration in terms of the interface temperature. The solution of this system of equations provides the interface values for  $f(0)$ ,  $Y_g(0)$ ,  $Y_l(0)$ ,  $h_g(0)$  and  $h_l(0)$ . More information on this interface algorithm is provided in Poblador-Ibanez and Sirignano [17].

The problem configurations solved in the present work are those from Davis et al. [24], where numerical results for a non-ideal two-phase laminar mixing layer using the system of partial differential equations are provided. Oxygen is chosen to be the pure gas species, while the liquid consists of pure  $n$ -decane. Mass fraction freestream conditions correspond to those previously discussed, with  $Y_1$  representing the pure gas species composition. Thus,  $Y_G = 1$  and  $Y_L = 0$ . Temperature freestream conditions are  $T_G = 550$  K and  $T_L = 450$  K. Using the thermodynamic model,  $h_G$  and  $h_L$  can be evaluated. To keep the boundary layer approximation valid, freestream conditions for the streamwise velocity vary among the different analyzed pressures. Their values are summarized in Table 1 and satisfy a critical Reynolds number based on the freestream velocity difference,  $\Delta u = u_L - u_G$ , and the gas freestream parameters of  $Re_L = 10,000$  at  $L = 0.01$  m. For a fixed mean velocity of 10 m/s,  $\Delta u$  needs to vary as the freestream gas density and viscosity change with pressure [24].

$p$ (bar)	$u_G$ (m/s)	$u_L$ (m/s)
10	7.673	12.327
50	9.525	10.475
100	9.755	10.246
150	9.830	10.170

Table 1: Freestream conditions for the streamwise component of the velocity field,  $u$ , at different ambient pressures [24].

The solution of the system of ordinary differential equations (ODE), Eqs. (18)-(20), is presented and compared to the results from Davis et al. [24] obtained from the system of partial differential equations (PDE). For visualization purposes, the results are non-dimensionalized by the liquid freestream conditions to provide a consistent comparison between different cases. The non-dimensional similarity variable and  $f$  function are, respectively,

$$\eta^* = \frac{\eta}{\sqrt{\frac{\rho_L \mu_L}{u_L}}} \quad (31)$$

and

$$f^* = \frac{f}{\sqrt{\rho_L \mu_L u_L}} \quad (32)$$

The non-dimensional second derivative of  $f$  (or velocity gradient) follows that

$$f''^* = \frac{f''}{\sqrt{\frac{u_L^3}{\rho_L \mu_L}}} \quad (33)$$



Any other variable is made dimensionless by dividing by the liquid freestream value (e.g.,  $h^* = h/h_L$  or  $f'^* = f'/u_L$ ). Note that  $Y$  is already non-dimensional. Furthermore, variables that are continuous across the interface (e.g.,  $f'$  and  $T$ ) are normalized as follows,

$$\theta_T(\eta) = \frac{T_L - T(\eta)}{T_L - T_G} \quad ; \quad \theta_u(\eta) = \frac{u_G - f'(\eta)}{u_G - u_L} \quad (34)$$

Figure 2 presents the non-dimensional solution of  $f^*$ ,  $f'^*$  and  $f''^*$ . Figure 2b shows how the interface velocity tends to be very close to the freestream liquid velocity. That is, the liquid phase is much more dense and viscous than the gas phase and it becomes hard for the slower gas stream to slow the liquid stream down. The solutions of  $Y$  and  $h^*$  are plotted in Figures 3 and 4.

As pressure increases well above the liquid critical pressure, the dissolution of the lighter gas species into the liquid phase is enhanced [16, 17] (see Figure 3a). This generates sharper fluid properties variations within the liquid phase, which can be responsible for the change in behavior seen in the liquid velocity gradient. As seen in Figure 2c, the velocity gradient behaves almost linearly within the liquid momentum mixing layer at subcritical pressures (i.e., 10 bar) where liquid density and viscosity remain fairly constant. However, as pressure increases well above the critical pressure of *n*-decane ( $p_c = 21.03$  bar), the velocity gradient shows an inflection point where its rate of change experiences a transition from a stronger deceleration of the liquid near the interface to a slower deceleration in a larger portion of the mixing layer.

The specific mixture enthalpy distribution is consistent with the increase of temperature in the liquid phase and the decrease of temperature in the gas phase. However, a wavy distribution is observed at 10 bar. A discussion based on a fundamental thermodynamic analysis is provided in Poblador-Ibanez and Sirignano [17]. Considering a mass element containing the whole mixing layer (liquid and gas), the mixing process is just an internal phenomenon. Negligible net heat flux crosses the boundaries of the mass element, therefore for a constant pressure process,  $\Delta H = Q|_p = 0$ . To compensate for the increase in enthalpy in the liquid phase, the gas phase enthalpy must decrease accordingly. At 10 bar, this requirement cannot be solely satisfied with a monotonic enthalpy distribution.

Figure 5 shows the non-dimensional continuous distributions of streamwise velocity,  $\theta_u$ , and temperature,  $\theta_T$ . As pressure increases and the gas dissolves more easily into the liquid phase, the interface velocity and temperature deviate further from the freestream liquid values. That is, as the liquid phase and the gas phase come closer together, the liquid loses inertia near the interface and the gas stream can slow it down more. Furthermore, the enhanced dissolution of the gas into the liquid increases the heat flux by diffusion into the liquid, raising its temperature.

The agreement between the solution of the self-similar system of ordinary differential equations (ODE) and the system of partial differential equations (PDE) is initially tested by comparing various profiles of different variables of interest. The PDE solution from Davis et al. [24] at a downstream position of  $x = 0.01$  m has been mapped from the  $(x, y)$  space to the  $\eta$  space for all four pressure cases. Figures 6 and 7 present these results for the non-dimensional distribution of continuous variables (i.e.,  $\theta_u$  and  $\theta_T$ ), where both methods are seen to concur for 50, 100 and 150 bar. At 10 bar, larger discrepancies are observed, especially in the gas phase distributions and the liquid temperature distribution.

Furthermore, the opposite mapping direction has been tested as well. That is, mapping the ODE solution from the  $\eta$  space to the  $(x, y)$  space. The main goal is to assess again the validity of both approaches and identify any numerical errors that might have arisen from the PDE-to-ODE domain mapping. Figures 8, 9 and 10 show the transverse profiles at various downstream locations of streamwise velocity,  $u$ , temperature,  $T$  and oxygen mass fraction,  $Y_1$ , at 150 bar. The profiles tend to collapse although some small deviations are seen depending on the variable and the fluid phase analyzed.

The results shown in Figures 6-10 suggest that the non-ideal two-phase laminar mixing layer equations do behave in a self-similar manner even though they are coupled to a complex thermodynamic model involving a cubic equation of state, high-pressure correlations used to evaluate transport properties and non-ideal thermodynamic principles.

To further compare the two approaches, the following lines examine the interface solution obtained with the system of ordinary differential equations and the steady interface solution obtained far downstream of the splitter plate with the system of partial differential equations. To assess the performance of the self-similar system of equations, the error of a given variable  $\phi$  between the solution of the ODE system and the PDE



system is defined as

$$E_\phi = \frac{|\phi_{\text{ODE}} - \phi_{\text{PDE}}|}{|\phi_{\text{PDE}}|} \quad (35)$$

which represents a relative deviation error from the PDE solution.

The interface values and the relative error of different variables of interest ( $U_\Gamma$ ,  $T_\Gamma$ , interface composition, etc.) obtained from the ODE solution and the PDE solution are shown in Tables 2-6. A very good agreement is seen, especially for the high pressure cases (i.e., 50, 100 and 150 bar). At subcritical pressures (i.e., 10 bar), errors are larger, following the trend observed in Figures 6 and 7.

Larger errors are observed when comparing the mass flux across the interface at a given location (see Table 6). At 100 and 150 bar, the predictions of the self-similar solution are in good agreement with the PDE solution, although errors are larger than for other interface properties. At 10 bar, the error is almost 30%. However, the error at 50 bar is very large ( $\approx 250\%$ ). This pressure case is very close to the transition point where phase change across the interface reverses from net vaporization to net condensation. That is, at 10 and 50 bar, net vaporization is occurring, while condensation dominates at higher pressures. This interface behavior and its implications on the liquid jet breakup are further discussed in [17, 21]. Sensitivity issues might arise close to this point, causing slight errors in the ODE solution or the PDE solution to produce large deviations in the mass flux across the interface. Therefore, a good comparison between both solutions is not possible. Nevertheless, both the ODE and the PDE solutions present the same trend in the interface behavior, which proves that both approaches are consistent.

## Conclusions

The non-ideal, two-phase, laminar mixing-layer equations have been reduced to a system of ordinary differential equations in terms of a similarity variable,  $\eta$ . The similarity transformation follows classical techniques used in compressible flows [26] and has been generalized to be implemented with any non-ideal thermodynamic model for the equation of state and phase equilibrium. In this work, the high-pressure thermodynamic model is based on a volume-corrected Soave-Redlich-Kwong cubic equation of state and other fundamental thermodynamic principles, coupled with high-pressure correlations to evaluate transport coefficients and phase equilibrium [24].

Good agreement between the self-similar solution and the solution of the system of partial differential equations is obtained, proving the validity of the self-similar approach. This is an important step towards reducing the complexity of the analysis of supercritical two-phase flows, while still capturing the main physics involved (e.g., enhanced diffusion in the liquid phase, phase change reversal at the interface). This type of approach can be helpful when used to implement realistic initial conditions to more complex flow simulations (i.e., high-pressure atomization).

The results show the existence of two phases at pressures above the critical pressure of any chemical component. It is seen that condensation can occur even though the gas is hotter and heat is conducting into the liquid.

## Acknowledgements

The authors are grateful for the support of the NSF grant with award number 1803833 and Dr. Ronald D. Joslin as Scientific Officer.

## References

- [1] W. O. H. Mayer and H. Tamura. *Journal of Propulsion and Power*, 12 (6):1137–1147, 1996.
- [2] W. O. H. Mayer, A. H. A. Schik, B. Vielle, C. Chauveau, I. Gökalp, and D. G. Talley. *Journal of Propulsion and Power*, 14 (5):835–842, 1998.
- [3] W. O. H. Mayer, A. H. A. Schik, M. Schaffler, and H. Tamura. *Journal of Propulsion and Power*, 16 (5):823–828, 2000.
- [4] B. Chehroudi, D. Talley, and E. Coy. *Physics of Fluids*, 14 (2):850–861, 2002.
- [5] B. Chehroudi, R. Cohn, and D. Talley. *International Journal of Heat and Fluid Flow*, 23 (5):554–563, 2002.



- [6] M. Oschwald, J.J. Smith, R. Branam, J. Hussong, A. Schik, B. Chehroudi, and D. Talley. *Combustion Science and Technology*, 178 (1-3):49–100, 2006.
- [7] B. Chehroudi. *International Journal of Aerospace Engineering*, 2012:121802, 2012.
- [8] C. Segal and A. Polikhov. *Physics of Fluids*, 20 (5):052101, 2008.
- [9] Z. Falgout, M. Rahm, D. Sedarsky, and M. Linne. *Fuel*, 168:14–21, 2016.
- [10] D.B. Spalding. *ARS Journal*, 29 (11):828–835, 1959.
- [11] D.E. Rosner. *AIAA Journal*, 5 (1):163–166, 1967.
- [12] K.C. Hsieh, J.S. Shuen, and V. Yang. *Combustion Science and Technology*, 76 (1-3):111–132, 1991.
- [13] J.P. Delplanque and W.A. Sirignano. *International Journal of Heat and Mass Transfer*, 36 (2):303–314, 1993.
- [14] V. Yang and J.S. Shuen. *Combustion Science and Technology*, 97 (4-6):247–270, 1994.
- [15] W.A. Sirignano, J.P. Delplanque, and F. Liu. *33rd Joint Propulsion Conference and Exhibit*, 1997.
- [16] A. Jordà Juanós and W. A. Sirignano. *25th ICDEERS*, Leeds, United Kingdom, August 2015.
- [17] J. Poblador-Ibanez and W. A. Sirignano. *International Journal of Heat and Mass Transfer*, 126:457–473, 2018.
- [18] R. N. Dahms and J. C. Oefelein. *Physics of Fluids*, 25 (9):092103, 2013.
- [19] R. N. Dahms and J. C. Oefelein. *Combustion and Flame*, 162 (10):3648–4657, 2015.
- [20] V. Yang. *Proceedings of the Combustion Institute*, 28 (1):925–942, 2000.
- [21] J. Poblador-Ibanez and W. A. Sirignano. *Proceedings of the ILASS-Americas 30th Annual Conference on Liquid Atomization and Spray Systems*, Tempe, AZ, Tempe, AZ, United States, May 2019.
- [22] M. Minniti, A. Ziaee, J. Trolinger, and D. Dunn-Rankin. *Atomization and Sprays*, 28 (6):565–579, 2018.
- [23] M. Minniti, A. Ziaee, D. Curran, J. Porter, T. Parker, and D. Dunn-Rankin. *Atomization and Sprays*, 29 (3):251–267, 2019.
- [24] B.W. Davis, J. Poblador-Ibanez, and W.A. Sirignano. *arXiv preprint arXiv:1912.01138*, 2019.
- [25] F.M. White and I. Corfield. *Viscous Fluid Flow*. McGraw-Hill New York, New York, 2006.
- [26] F.A. Williams. *Combustion Theory*. CRC Press, 2018.
- [27] C.A. Kennedy and T.B. Gatski. *Physics of Fluids*, 6 (2):662–673, 1994.
- [28] P. He and A. F. Ghoniem. *Journal of Computational Physics*, 332:316–332, 2017.
- [29] H. Lin, Y.-Y. Duan, T. Zhang, and Z.-M. Huang. *Industrial & Engineering Chemistry Research*, 45 (5):1829–1839, 2006.
- [30] G. Soave. *Chemical Engineering Science*, 27 (6):1197–1203, 1972.
- [31] J.M. Prausnitz and F.W. Tavares. *AIChE Journal*, 50 (4):739–761, 2004.
- [32] B.E. Poling, J.M. Prausnitz, O. John-Paul, and R.C. Reid. *The Properties of Gases and Liquids*. McGraw Hill, New York, 2001.
- [33] T.H. Chung, M. Ajlan, L.L. Lee, and K.E. Starling. *Industrial & Engineering Chemistry Research*, 27 (4):671–679, 1988.
- [34] A. Leahy-Dios and A. Firoozabadi. *AIChE Journal*, 53 (11):2932–2939, 2007.



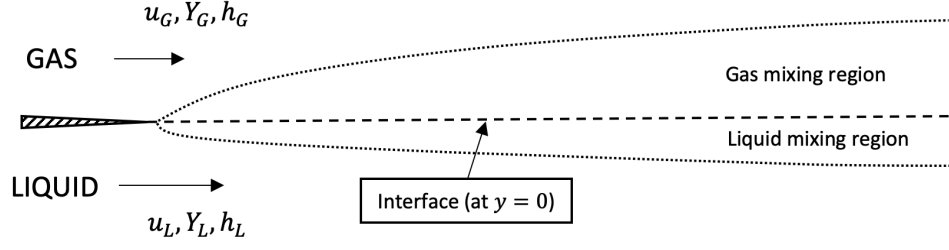


Figure 1: Sketch of the mixing layer problem between a liquid stream and a gas stream. The liquid-gas interface or dividing streamline is assumed to be fixed at  $y = 0$  m as discussed in [24].

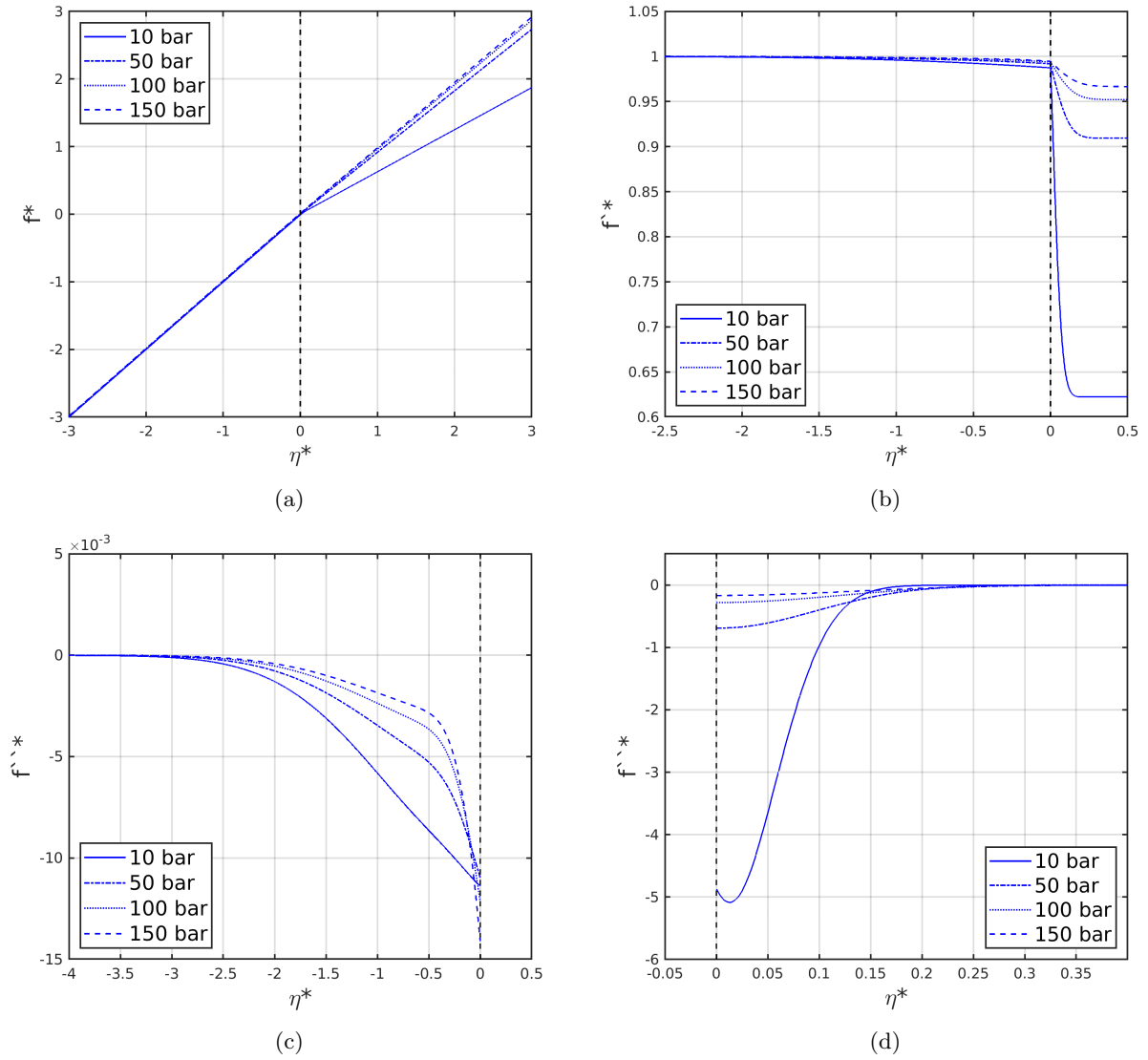
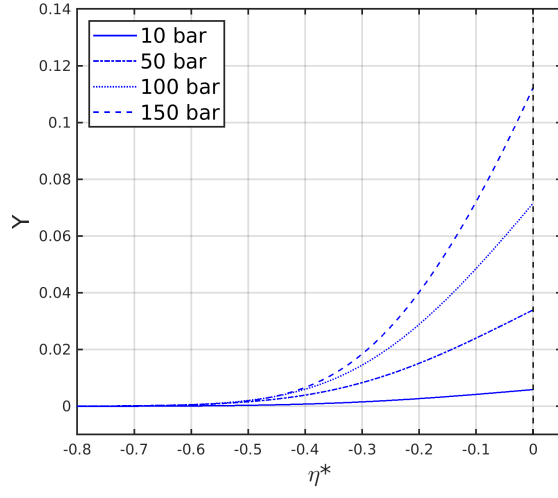
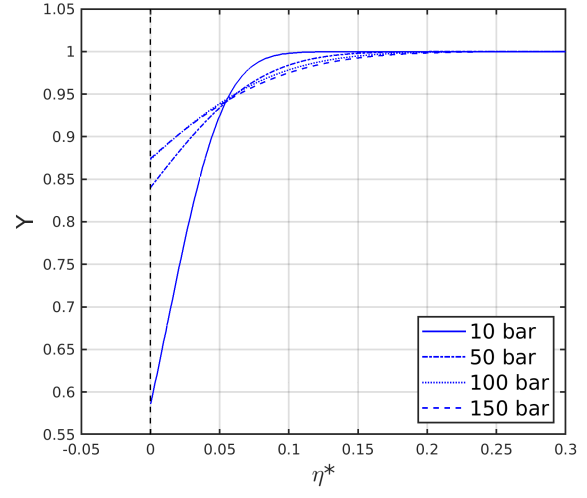


Figure 2: Solution of the self-similar system of ordinary differential equations. (a)  $f^*$ ; (b)  $f'^*$ ; (c)  $f''^*$  in the liquid phase; (d)  $f'''^*$  in the gas phase.



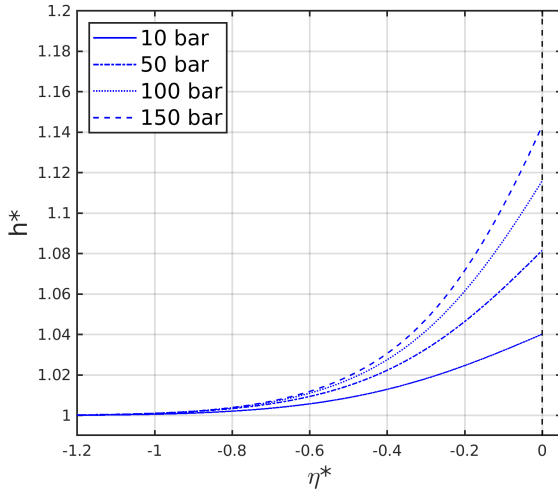


(a)

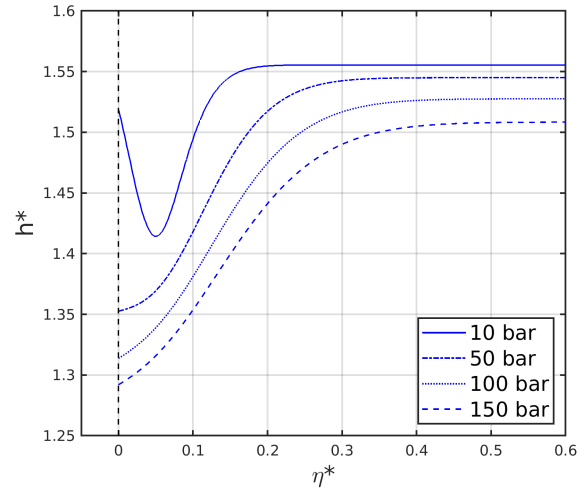


(b)

Figure 3: Solution of the self-similar system of ordinary differential equations. (a)  $Y$  in the liquid phase; (b)  $Y$  in the gas phase. The plotted mass fraction represents the oxygen mass fraction (i.e.,  $Y = Y_1 = Y_{O_2}$ ).



(a)



(b)

Figure 4: Solution of the self-similar system of ordinary differential equations. (a)  $h^*$  in the liquid phase; (b)  $h^*$  in the gas phase.



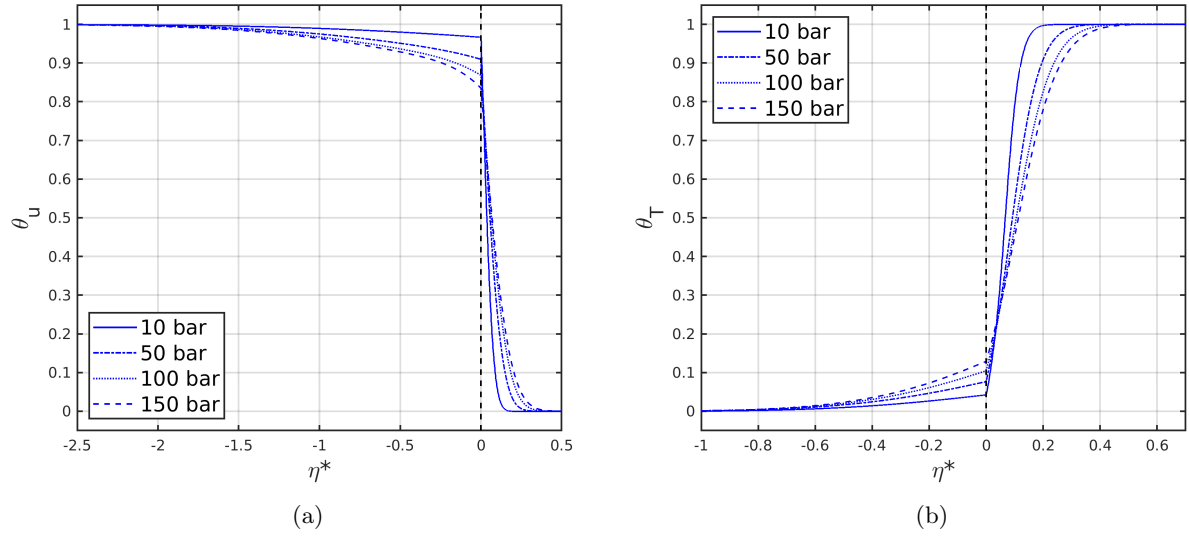


Figure 5: Solution of the self-similar system of ordinary differential equations. (a)  $\theta_u$ ; (b)  $\theta_T$ .

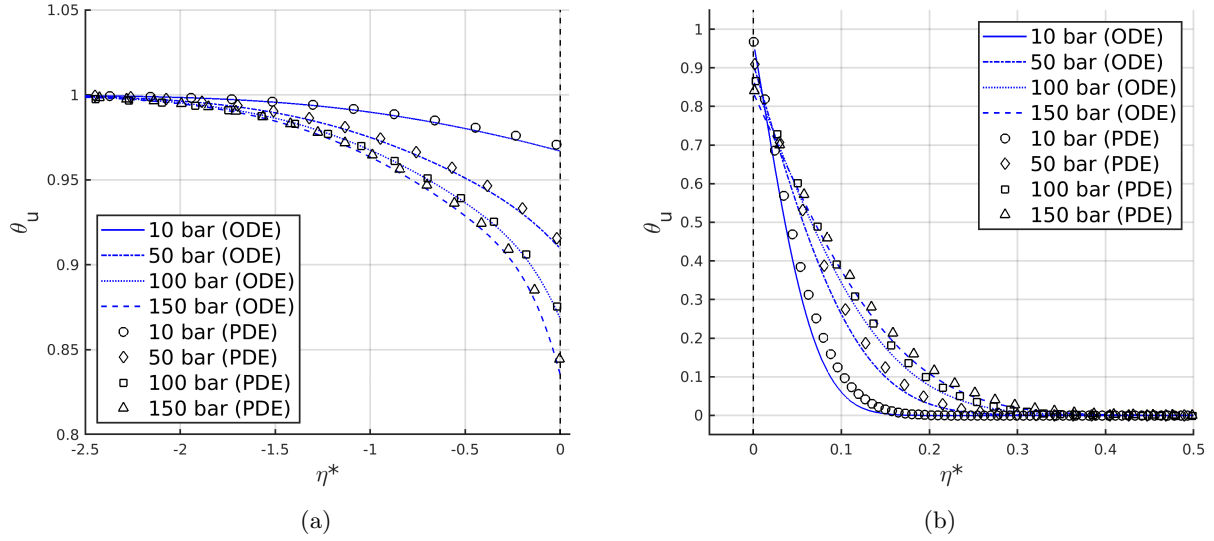


Figure 6: Comparison between the solution of the system of ordinary differential equations (ODE) and the solution of the system of partial differential equations (PDE) mapped from  $(x,y)$  to  $\eta$ . (a)  $\theta_u$  in the liquid phase; (b)  $\theta_u$  in the gas phase.



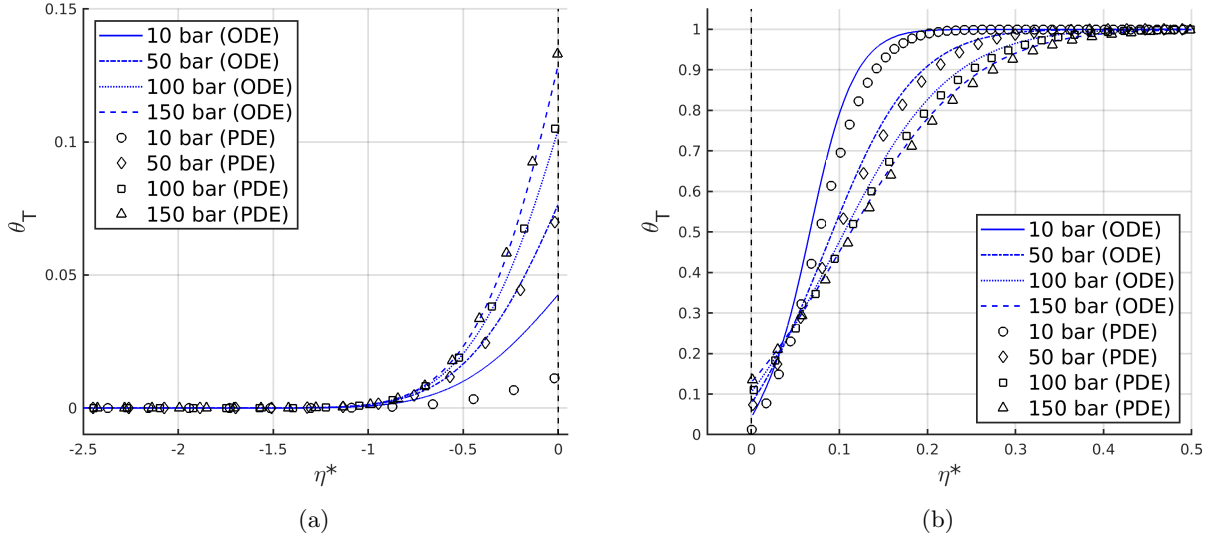


Figure 7: Comparison between the solution of the system of ordinary differential equations (ODE) and the solution of the system of partial differential equations (PDE) mapped from  $(x,y)$  to  $\eta$ . (a)  $\theta_T$  in the liquid phase; (b)  $\theta_T$  in the gas phase.

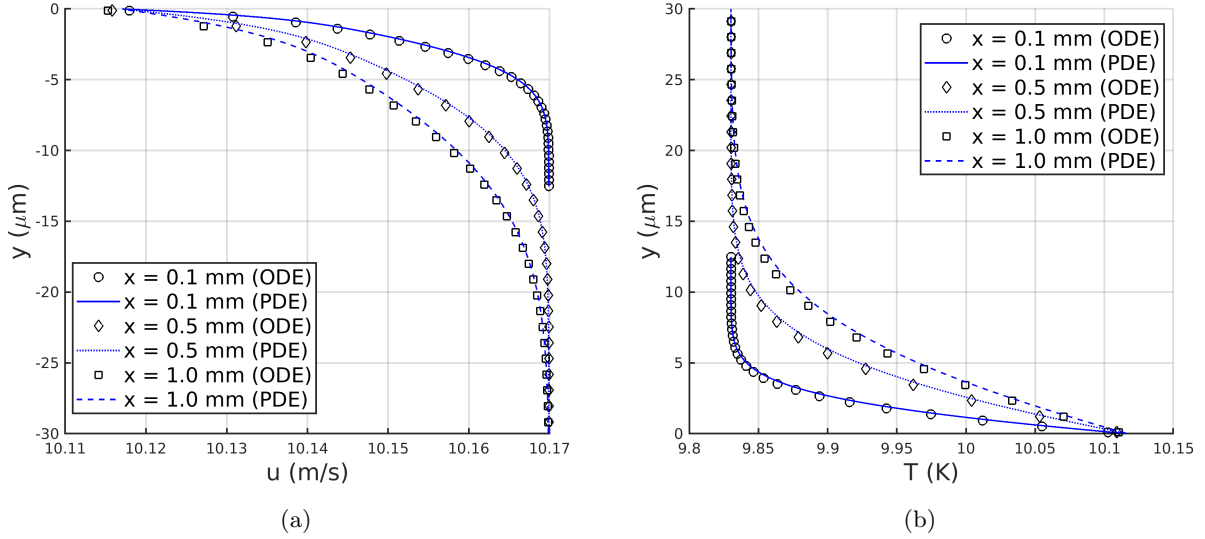


Figure 8: Comparison between the solution at 150 bar of the system of ordinary differential equations (ODE) and the solution of the system of partial differential equations (PDE) mapped from  $\eta$  to  $(x,y)$ . (a)  $u$  in the liquid phase; (b)  $u$  in the gas phase.



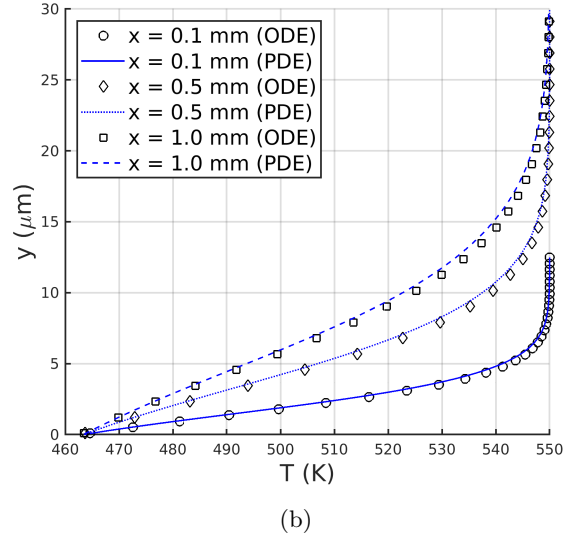
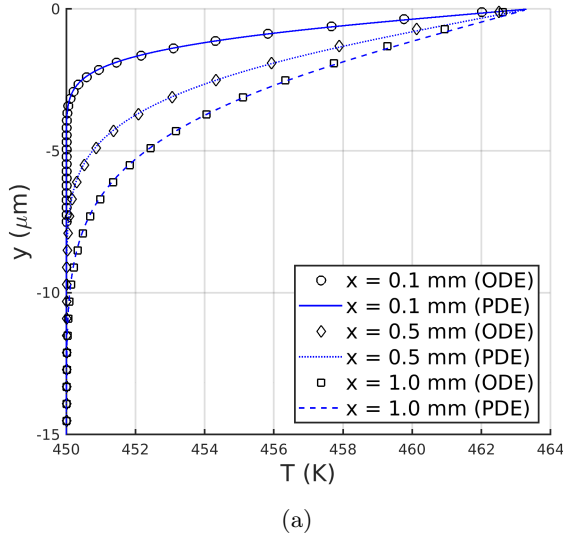


Figure 9: Comparison between the solution at 150 bar of the system of ordinary differential equations (ODE) and the solution of the system of partial differential equations (PDE) mapped from  $\eta$  to  $(x,y)$ . (a)  $T$  in the liquid phase; (b)  $T$  in the gas phase.

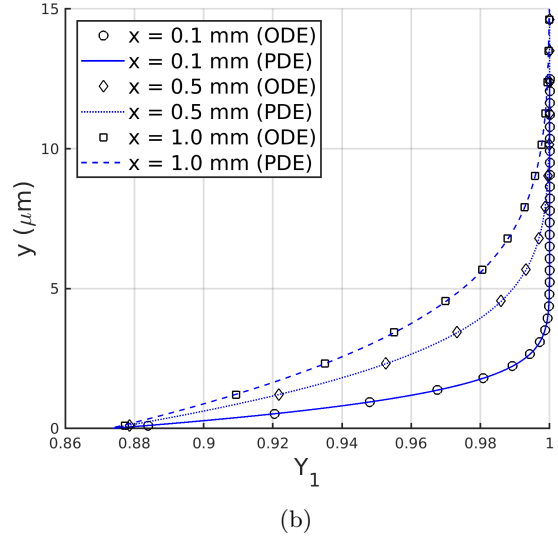
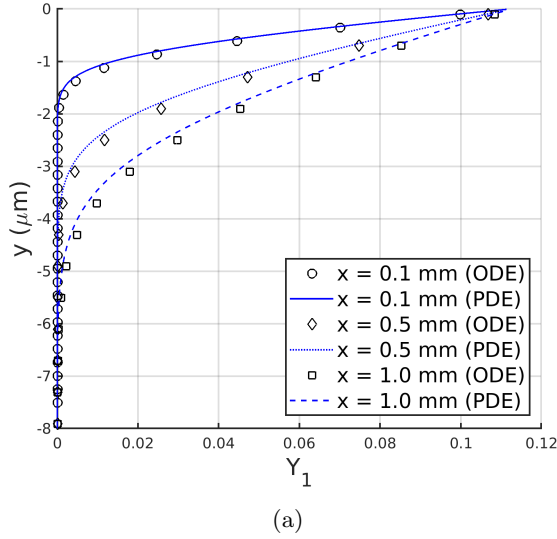


Figure 10: Comparison between the solution at 150 bar of the system of ordinary differential equations (ODE) and the solution of the system of partial differential equations (PDE) mapped from  $\eta$  to  $(x,y)$ . (a)  $Y_1$  in the liquid phase; (b)  $Y_1$  in the gas phase. The plotted mass fraction represents the oxygen mass fraction (i.e.,  $Y_1 = Y_{O_2}$ ).



$p$ (bar)	$U_{\Gamma,\text{ODE}}$ (m/s)	$U_{\Gamma,\text{PDE}}$ (m/s)	$E_{U_{\Gamma}}$ (%)	$T_{\Gamma,\text{ODE}}$ (K)	$T_{\Gamma,\text{PDE}}$ (K)	$E_{T_{\Gamma}}$ (%)
10	12.174	12.190	0.1313	454.261	451.153	0.6889
50	10.389	10.394	0.0481	457.653	457.119	0.1168
100	10.181	10.184	0.0295	460.452	460.708	0.0556
150	10.114	10.117	0.0297	462.890	463.382	0.1062

Table 2: Comparison of the interface velocity,  $U_{\Gamma}$ , and equilibrium temperature,  $T_{\Gamma}$ , between the solutions obtained using the system of ordinary differential equations (ODE) and the system of partial differential equations (PDE).

$p$ (bar)	$Y_{g,O_2,\text{ODE}}$	$Y_{g,O_2,\text{PDE}}$	$E_{Y_{g,O_2}}$ (%)	$Y_{l,O_2,\text{ODE}}$	$Y_{l,O_2,\text{PDE}}$	$E_{Y_{l,O_2}}$ (%)
10	0.5860	0.6072	3.491	0.0059	0.0060	1.667
50	0.8401	0.8420	0.226	0.0339	0.0339	$\sim 0$
100	0.8732	0.8726	0.069	0.0715	0.0715	$\sim 0$
150	0.8741	0.8729	0.137	0.1123	0.1123	$\sim 0$

Table 3: Comparison of the interface equilibrium composition on each phase,  $Y_{g,O_2}$  and  $Y_{l,O_2}$ , between the solutions obtained using the system of ordinary differential equations (ODE) and the system of partial differential equations (PDE).

$p$ (bar)	$\rho_{g,\text{ODE}}$ (kg/m <sup>3</sup> )	$\rho_{g,\text{PDE}}$ (kg/m <sup>3</sup> )	$E_{\rho_g}$ (%)	$\rho_{l,\text{ODE}}$ (kg/m <sup>3</sup> )	$\rho_{l,\text{PDE}}$ (kg/m <sup>3</sup> )	$E_{\rho_l}$ (%)
10	12.622	12.392	1.856	590.485	593.843	0.565
50	47.934	47.915	0.040	580.350	580.960	0.105
100	91.435	91.435	$\sim 0$	572.964	572.604	0.063
150	134.396	134.381	0.011	565.565	564.875	0.122

Table 4: Comparison of the interface equilibrium mixture densities on each phase,  $\rho_g$  and  $\rho_l$ , between the solutions obtained using the system of ordinary differential equations (ODE) and the system of partial differential equations (PDE).

$p$ (bar)	$h_{g,\text{ODE}}$ (kJ/kg)	$h_{g,\text{PDE}}$ (kJ/kg)	$E_{h_g}$ (%)	$h_{l,\text{ODE}}$ (kJ/kg)	$h_{l,\text{PDE}}$ (kJ/kg)	$E_{h_l}$ (%)
10	496.990	488.192	1.802	340.530	331.724	2.655
50	444.700	443.749	0.214	355.620	354.116	0.425
100	435.700	436.109	0.094	370.160	370.867	0.191
150	433.110	433.862	0.173	383.250	384.590	0.348

Table 5: Comparison of the interface equilibrium mixture enthalpies on each phase,  $h_g$  and  $h_l$ , between the solutions obtained using the system of ordinary differential equations (ODE) and the system of partial differential equations (PDE).

$p$ (bar)	$\dot{\omega}_{\text{ODE}}$ (kg/ms <sup>2</sup> )	$\dot{\omega}_{\text{PDE}}$ (kg/ms <sup>2</sup> )	$E_{\dot{\omega}}$ (%)
10	0.0849	0.0665	28.091
50	0.00511	0.00144	254.86
100	-0.0573	-0.0590	2.8814
150	-0.115	-0.117	1.7094

Table 6: Comparison of the net mass flux across the interface,  $\dot{\omega}$ , at the downstream location  $x = \bar{x} = 0.01$  m between the solutions obtained using the system of ordinary differential equations (ODE) and the system of partial differential equations (PDE).